

# Synthesis and selected properties of a new solid solution in the $\text{Zn}_2\text{FeV}_3\text{O}_{11}$ – $\text{Mg}_2\text{FeV}_3\text{O}_{11}$ system

A. Blonska-Tabero · E. Filipek · P. Tabero

Bretsznajder Special Chapter

© The Author(s) 2012. This article is published with open access at Springerlink.com

**Abstract** The binary  $\text{Zn}_2\text{FeV}_3\text{O}_{11}$ – $\text{Mg}_2\text{FeV}_3\text{O}_{11}$  system has been studied by XRD, DTA, IR, and SEM methods. A new continuous substitution solid solution with the formula  $\text{Zn}_{2-x}\text{Mg}_x\text{FeV}_3\text{O}_{11}$  has been obtained by high-temperature synthesis. The DTA investigations were used to choose the heating temperatures as well as for determination of thermal stability of the new triclinic phase. The influence of the degree of  $\text{Mg}^{2+}$  ion incorporation on the unit cell volume as well as on the position of the IR absorption bands of the solid solution have been determined. The morphology of crystals of the new phase is presented.

**Keywords** Solid solution  $\text{Zn}_{2-x}\text{Mg}_x\text{FeV}_3\text{O}_{11}$  · DTA · XRD · IR

## Introduction

Physicochemical properties of solid solutions are possible to modify, which is very important for designing of new functional materials. The knowledge on the influence of the change of composition of the solid solutions on their properties enable to synthesize the phases with desirable thermal, electric, magnetic or catalytic properties. A literature scan has shown that obtaining of new catalysts for oxidative dehydrogenation of organic compounds is at present still a challenging problem. Some vanadates(V) catalyze these reactions and their activity is associated with the presence, in

their structure, of isolated  $\text{VO}_4$  tetrahedra (orthovanadates) or corner sharing  $\text{VO}_4$  tetrahedra in the  $\text{V}_2\text{O}_7$  units (pyrovanadates) [1–3]. In search of new phases, interesting from point of view of catalysis, reactivity of iron(III) orthovanadate(V) towards pyrovanadates(V)  $\text{M}_2\text{V}_2\text{O}_7$  ( $\text{M} = \text{Co}, \text{Mg}, \text{Ni}, \text{Pb}, \text{Zn}$ ) has been investigated and a series of compounds with the general formula  $\text{M}_2\text{FeV}_3\text{O}_{11}$  has been obtained [4–8]. Phases  $\text{Zn}_2\text{FeV}_3\text{O}_{11}$  and  $\text{Mg}_2\text{FeV}_3\text{O}_{11}$  are isostructural [8, 9] and, what is very important, in their structures isolated  $\text{VO}_4$  tetrahedra can be distinguished. Considering approximate values of  $\text{Zn}^{2+}$  and  $\text{Mg}^{2+}$  radii (0.074 and 0.072 nm, respectively) in  $\text{MO}_6$  ( $\text{M} = \text{Zn}, \text{Mg}$ ) polyhedra [10] it can be expected that  $\text{Zn}_2\text{FeV}_3\text{O}_{11}$  and  $\text{Mg}_2\text{FeV}_3\text{O}_{11}$  will form the substitution solid solution. Formation of such solution has been stated in the another vanadates systems [11–13]. The synthesis of a new solid solution forming in the system  $\text{Zn}_2\text{FeV}_3\text{O}_{11}$ – $\text{Mg}_2\text{FeV}_3\text{O}_{11}$  enable to modify physicochemical properties of phases with potential catalytic properties.

The aim of presented study is to find out whether the compounds,  $\text{Zn}_2\text{FeV}_3\text{O}_{11}$  and  $\text{Mg}_2\text{FeV}_3\text{O}_{11}$ , form a solid solution and if it is so—what the range of their solubility is. The second point of the study is to investigate the influence of degree of a foreign ion incorporation in the crystal lattice of the matrix on some of physicochemical properties of obtained new solid solution.

## Experimental

The following reactants were used in experiments: ZnO (p.a., Ubichem, England),  $3\text{MgCO}_3 \cdot \text{Mg}(\text{OH})_2 \cdot 3\text{H}_2\text{O}$  (p.a., POCh, Poland),  $\text{V}_2\text{O}_5$  (p.a., Riedel-de Haën, Germany),  $\alpha\text{-Fe}_2\text{O}_3$  (p.a., POCh, Poland),  $\text{Mg}_2\text{FeV}_3\text{O}_{11}$ , and  $\text{Zn}_2\text{FeV}_3\text{O}_{11}$ . Syntheses of  $\text{Mg}_2\text{FeV}_3\text{O}_{11}$  and  $\text{Zn}_2\text{FeV}_3\text{O}_{11}$  were performed during heating the stoichiometric mixtures of  $\text{V}_2\text{O}_5$  and  $\alpha$ -

A. Blonska-Tabero (✉) · E. Filipek · P. Tabero  
Department of Inorganic and Analytical Chemistry,  
West Pomeranian University of Technology, Szczecin,  
Al. Piastow 42, 71-065 Szczecin, Poland  
e-mail: abtab@zut.edu.pl

Fe<sub>2</sub>O<sub>3</sub> with 3MgCO<sub>3</sub>·Mg(OH)<sub>2</sub>·3H<sub>2</sub>O or with ZnO, respectively, in the following stages: 570 °C(20 h) × 2 + 600 °C(20 h) + 680 °C(20 h).

Syntheses were carried out by the standard method of calcining samples described inter alia in the papers [14–19]. Mixtures of appropriate portions of the reagents were homogenized by grinding in an automated agate mortar and they were heated in air for several 20-h stages in the temperature range 760–900 °C. The exact conditions of heating are given in Table 1. To avoid the melting of the samples they were heated at temperatures several dozen of °C lower than their melting temperatures. The onset temperature of the first endothermic effect recorded in DTA curve of given sample was taken as the melting temperature of this sample. Accuracy of reading these temperatures was determined by repetitions. After each heating stage the samples were gradually cooled down in furnace to room temperature, ground and examined by X-ray diffraction method with respect to their composition. This procedure was repeated until the results of investigations of the samples, by XRD and DTA methods, did not change after two consecutive heating stages.

The DTA investigations were performed in static air atmosphere using the Paulik–Paulik–Erdey type derivatograph (MOM, Hungary). Five hundred milligram of each investigated sample was placed in a quartz crucible and was heated from room temperature up to ~ 1,050 °C at a heating rate of 10° min<sup>-1</sup>.

The phases in each sample were identified from XRD patterns obtained using a HZG-4/A2 diffractometer (Carl Zeiss, Germany) with CuK<sub>α</sub>/Ni radiation. The phase analyses were conducted basing on the XRD characteristics contained in the PDF cards and on the data presented in study [9]. The powder diffraction patterns of selected samples were indexed by means of the Refinement program. The internal standard was α-Al<sub>2</sub>O<sub>3</sub>.

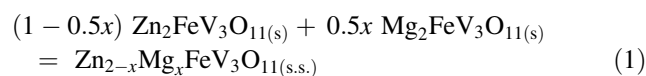
IR spectroscopic measurements were conducted with the use of the spectrometer Specord M 80 (Carl Zeiss, Germany), applying the technique of pressing pellets of investigated sample with KBr at a weight ratio 1:300.

The morphology of the crystals was observed by means of an electron scanning microscope (JSM-1600, Jeol, Japan).

## Results and discussion

### Synthesis and XRD analysis results

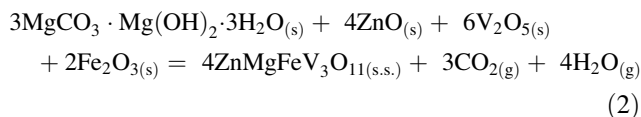
Nine mixtures of separately obtained compounds, Zn<sub>2</sub>FeV<sub>3</sub>O<sub>11</sub> and Mg<sub>2</sub>FeV<sub>3</sub>O<sub>11</sub>, were prepared for the investigation, with their composition covering the whole component concentration range of the system under study. Table 1 presents the composition of the initial mixtures, their heating conditions and phase composition of these samples after their final heating stage. XRD analysis results of all samples at an equilibrium state show them to be monophasic. Based on the obtained diffraction patterns it can be concluded that in the Zn<sub>2</sub>FeV<sub>3</sub>O<sub>11</sub>–Mg<sub>2</sub>FeV<sub>3</sub>O<sub>11</sub> system a continuous substitution solid solution is formed. Its general formula can be written both as Zn<sub>2–x</sub>Mg<sub>x</sub>FeV<sub>3</sub>O<sub>11</sub> and as Mg<sub>2–x</sub>Zn<sub>x</sub>FeV<sub>3</sub>O<sub>11</sub>. In order to depict the changes of some properties of the new phase, its formula was always written as Zn<sub>2–x</sub>Mg<sub>x</sub>FeV<sub>3</sub>O<sub>11</sub>. Formation of the new solid solution follows therefore according to the equation:



The synthesis of the solid solution with the formula ZnMgFeV<sub>3</sub>O<sub>11</sub> was also carried out according to the another equation, i.e.:

**Table 1** The composition of the initial mixtures, their heating conditions and the formula of the obtained solid solution

No.	<i>x</i>	Composition of initial mixtures, mol%		Heating conditions	Formula of solid solution, Zn <sub>2–x</sub> Mg <sub>x</sub> FeV <sub>3</sub> O <sub>11</sub>
		Zn <sub>2</sub> FeV <sub>3</sub> O <sub>11</sub>	Mg <sub>2</sub> FeV <sub>3</sub> O <sub>11</sub>		
1.	0.2	90.00	10.00	760 °C(20 h) + 830 °C(20 h) × 2	Zn <sub>1.8</sub> Mg <sub>0.2</sub> FeV <sub>3</sub> O <sub>11</sub>
2.	0.4	80.00	20.00		Zn <sub>1.6</sub> Mg <sub>0.4</sub> FeV <sub>3</sub> O <sub>11</sub>
3.	0.6	70.00	30.00		Zn <sub>1.4</sub> Mg <sub>0.6</sub> FeV <sub>3</sub> O <sub>11</sub>
4.	0.8	60.00	40.00	760 °C(20 h) + 860 °C(20 h) × 2	Zn <sub>1.2</sub> Mg <sub>0.8</sub> FeV <sub>3</sub> O <sub>11</sub>
5.	1.0	50.00	50.00		ZnMgFeV <sub>3</sub> O <sub>11</sub>
6.	1.2	40.00	60.00		Zn <sub>0.8</sub> Mg <sub>1.2</sub> FeV <sub>3</sub> O <sub>11</sub>
7.	1.4	30.00	70.00	760 °C(20 h) + 900 °C(20 h) × 2	Zn <sub>0.6</sub> Mg <sub>1.4</sub> FeV <sub>3</sub> O <sub>11</sub>
8.	1.6	20.00	80.00		Zn <sub>0.4</sub> Mg <sub>1.6</sub> FeV <sub>3</sub> O <sub>11</sub>
9.	1.8	10.00	90.00		Zn <sub>0.2</sub> Mg <sub>1.8</sub> FeV <sub>3</sub> O <sub>11</sub>



The stoichiometric mixture of the reactants was heated in the following stages: 580 °C(20 h) × 2 + 760 °C (20 h) + 860 °C(20 h) × 2. The calcination at 580 °C enabled a total consumption of vanadium(V) oxide ( $t_m = 650 \pm 5$  °C) without its melting. The powder diffraction pattern of the sample obtained after its last heating stage did not differ from that obtained for the sample 5 being at equilibrium (Table 1).

Formation of the new solid solution has been corroborated by the next presented investigations.

### Unit cell parameters

In the further stage of research, powder diffraction patterns of the obtained solid solution were indexed. Table 2 shows parameters and volumes of unit cells of pure  $\text{Zn}_2\text{FeV}_3\text{O}_{11}$  and  $\text{Mg}_2\text{FeV}_3\text{O}_{11}$  phases as well as of the new solid solution  $\text{Zn}_{2-x}\text{Mg}_x\text{FeV}_3\text{O}_{11}$  for  $x = 0.4, 1.0$  and  $1.6$ . The values of unit cell parameters of  $\text{Zn}_2\text{FeV}_3\text{O}_{11}$  and  $\text{Mg}_2\text{FeV}_3\text{O}_{11}$  calculated in the frame of this study (Table 2) are in accord with literature data [8, 9]. Analysis of the data presented in Table 2 has pointed out that with the increasing degree of  $\text{Mg}^{2+}$  ion incorporation into the  $\text{Zn}_2\text{FeV}_3\text{O}_{11}$  lattice, a values of parameters a and b as well as the unit cell volumes decrease in comparison to the pure solid solution matrix, i.e.,  $\text{Zn}_2\text{FeV}_3\text{O}_{11}$ . On the other hand values of the unit cell parameter c increase with increasing magnesium content. Taking under consideration, that the  $\text{Mg}^{2+}$  ion radius (0.072 nm) is shorter than this, characteristic for  $\text{Zn}^{2+}$  one (0.074 nm) [10], it is an unusual and interesting case. Wang and co-workers [9] have suggested, that significant difference in the degree of  $\text{M}(2)\text{O}_6$  octahedra distortion between these two phases is responsible for the unusual change in unit cell parameters of these phases. The results of our analysis of structural data presented in [9] indicate that substitution of magnesium for zinc in the crystal lattice of  $\text{Zn}_2\text{FeV}_3\text{O}_{11}$  strongly affects the bond lengths in  $\text{M}(2)\text{O}_6$  and  $\text{M}(3)\text{O}_5$  polyhedra. It

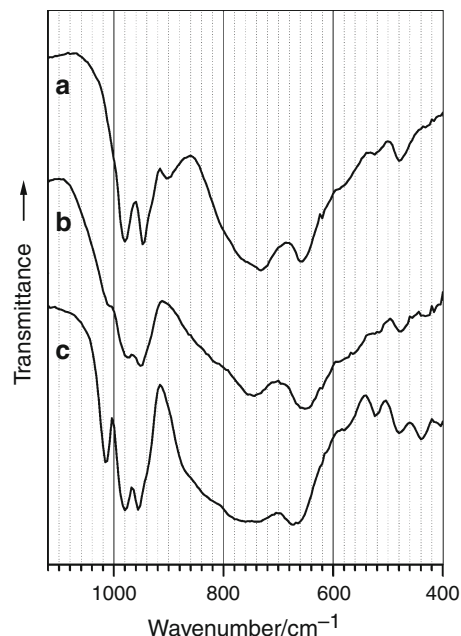


**Fig. 1** IR spectra of: a  $\text{Zn}_2\text{FeV}_3\text{O}_{11}$ , b  $\text{ZnMgFeV}_3\text{O}_{11}$ , c  $\text{Mg}_2\text{FeV}_3\text{O}_{11}$

reduces the length of the longest  $\text{M}(2)\text{--O}(10)$  bond in  $\text{M}(2)\text{O}_6$  octahedron which is parallel to a direction and the length of the longest bonds  $\text{M}(3)\text{--O}(4)$  and  $\text{M}(3)\text{--O}(5)$  in  $\text{M}(3)\text{O}_5$  trigonal bipyramid which are parallel to b direction. Thus, incorporation of more and more amounts of  $\text{Mg}^{2+}$  ions into the crystal lattice of  $\text{Zn}_2\text{FeV}_3\text{O}_{11}$  is responsible for a and b unit cell parameters decrease. On the other hand shortening of these bonds affects the heights of appropriate polyhedral, directed parallel to c direction, enlarging unit cell parameter c of the solid solution phases.

### IR spectroscopy

The phases  $\text{Zn}_2\text{FeV}_3\text{O}_{11}$  and  $\text{Mg}_2\text{FeV}_3\text{O}_{11}$  as well as solid solution  $\text{Zn}_{2-x}\text{Mg}_x\text{FeV}_3\text{O}_{11}$  were also subjected to an investigation with the aid of infrared spectroscopy (IR). Figure 1 shows the IR spectra of pure  $\text{Zn}_2\text{FeV}_3\text{O}_{11}$  (curve a), solid solution with the formula  $\text{ZnMgFeV}_3\text{O}_{11}$

**Table 2** The unit cell parameters and unit cell volumes of  $\text{Zn}_2\text{FeV}_3\text{O}_{11}$  and  $\text{Mg}_2\text{FeV}_3\text{O}_{11}$  compounds and of the solid solution  $\text{Zn}_{2-x}\text{Mg}_x\text{FeV}_3\text{O}_{11}$  for  $x = 0.4, 1.0, 1.6$

Formula	a/nm	b/nm	c/nm	$\alpha^\circ$	$\beta^\circ$	$\gamma^\circ$	V/nm <sup>3</sup>
$\text{Zn}_2\text{FeV}_3\text{O}_{11}$	0.6458(3)	0.6842(3)	0.9998(3)	97.53(4)	102.62(4)	101.30(4)	0.4157(3)
$\text{Zn}_{1.6}\text{Mg}_{0.4}\text{FeV}_3\text{O}_{11}$	0.6454(2)	0.6834(2)	1.0018(2)	97.52(2)	102.83(3)	101.38(3)	0.4152(2)
$\text{ZnMgFeV}_3\text{O}_{11}$	0.6445(2)	0.6823(2)	1.0043(3)	97.46(3)	103.04(4)	101.40(4)	0.4147(2)
$\text{Zn}_{0.4}\text{Mg}_{1.6}\text{FeV}_3\text{O}_{11}$	0.6438(3)	0.6812(2)	1.0072(3)	97.39(2)	103.29(3)	101.42(3)	0.4143(3)
$\text{Mg}_2\text{FeV}_3\text{O}_{11}$	0.6436(2)	0.6804(2)	1.0088(3)	97.40(3)	103.46(4)	101.45(4)	0.4139(2)

(curve b), and pure  $\text{Mg}_2\text{FeV}_3\text{O}_{11}$  (curve c). All recorded IR spectra of  $\text{Zn}_{2-x}\text{Mg}_x\text{FeV}_3\text{O}_{11}$  phase are similar to one another (and to IR spectra of  $\text{Zn}_2\text{FeV}_3\text{O}_{11}$  and  $\text{Mg}_2\text{FeV}_3\text{O}_{11}$ ) however, broadening of absorption bands is observed in comparison to the IR spectra of the  $\text{Zn}_2\text{FeV}_3\text{O}_{11}$  and  $\text{Mg}_2\text{FeV}_3\text{O}_{11}$  (Fig. 1, curve b). This broadening is undoubtedly due to an appearance of numerous new M–O bonds with their lengths differing from those ones occurring in the structure of  $\text{Zn}_2\text{FeV}_3\text{O}_{11}$  and  $\text{Mg}_2\text{FeV}_3\text{O}_{11}$  [20]. With increasing the incorporation extent of the smaller and lighter  $\text{Mg}^{2+}$  ions into the structure of  $\text{Zn}_2\text{FeV}_3\text{O}_{11}$  a shift of the respective absorption bands towards higher wave numbers is observed.

The IR spectrum of  $\text{ZnMgFeV}_3\text{O}_{11}$  contains two broad absorption bands. The first one spreading over the range of  $1,070\text{--}920\text{ cm}^{-1}$  have two maxima at  $978$  and  $950\text{ cm}^{-1}$  and two shoulders at  $1,010$  and  $934\text{ cm}^{-1}$ . At this wave number range one can expect the occurrence of absorption bands related with stretching vibrations of V–O bonds in highly distorted  $\text{VO}_4$  and  $\text{VO}_5$  polyhedra [5, 9, 21–23]. A shoulder at  $1,010\text{ cm}^{-1}$  most probably can be ascribed to stretching vibration of the shortest V–O bond in  $\text{VO}_5$  trigonal bipyramids characteristic for crystal structure of both  $\text{Zn}_2\text{FeV}_3\text{O}_{11}$  and  $\text{Mg}_2\text{FeV}_3\text{O}_{11}$  [9, 21]. The second band covering the range of  $920\text{--}400\text{ cm}^{-1}$  is very broad. It has two maxima at  $744$  and  $650\text{ cm}^{-1}$  and two shoulders at  $822$  and  $570\text{ cm}^{-1}$ . Band lying within the wave number range of  $920\text{--}600\text{ cm}^{-1}$  may be related with the stretching vibrations in moderately distorted  $\text{VO}_4$  tetrahedra [5, 21–23]. On the other hand, absorption bands below  $600\text{ cm}^{-1}$  can be ascribed to stretching vibrations in  $\text{ZnO}_x$ ,  $\text{MgO}_x$ , and  $\text{FeO}_x$  polyhedra and to bending vibrations in  $\text{VO}_x$  polyhedra [5, 9, 20, 22–24]. They can have also a mixed character.

### Thermal stability

Pure  $\text{Zn}_2\text{FeV}_3\text{O}_{11}$  and  $\text{Mg}_2\text{FeV}_3\text{O}_{11}$  phases as well as the solid solution  $\text{Zn}_{2-x}\text{Mg}_x\text{FeV}_3\text{O}_{11}$  for  $x = 0.2, 0.4, 0.6, 0.8, 1.0, 1.2, 1.4, 1.6, 1.8$  were investigated by DTA method. According to the obtained results  $\text{Zn}_2\text{FeV}_3\text{O}_{11}$  melts at  $865 \pm 5\text{ }^\circ\text{C}$ , whereas temperature of  $\text{Mg}_2\text{FeV}_3\text{O}_{11}$  melting amounts to  $1005 \pm 5\text{ }^\circ\text{C}$ . DTA curves of the obtained solid solution reveal only one endothermic effect. Its onset temperature increases with increasing the content of  $\text{Mg}^{2+}$  ions.

The endothermic effect recorded on the DTA curve of  $\text{Zn}_{2-x}\text{Mg}_x\text{FeV}_3\text{O}_{11}$  for  $x = 0.2, 0.4, 0.6, 0.8, 1.0, 1.2, 1.4, 1.6,$  and  $1.8$  has its onset at  $885 \pm 5, 895 \pm 5, 905 \pm 5, 920 \pm 5, 935 \pm 5, 950 \pm 5, 965 \pm 5, 980 \pm 5,$  and  $990 \pm 5\text{ }^\circ\text{C}$ , respectively. Therefore, the onset temperature of the registered effect is always higher than the melting temperature of pure  $\text{Zn}_2\text{FeV}_3\text{O}_{11}$  and lower than the melting temperature of pure  $\text{Mg}_2\text{FeV}_3\text{O}_{11}$ . Figure 2 shows fragments of DTA curves of solid solution  $\text{Zn}_{2-x}\text{Mg}_x\text{FeV}_3\text{O}_{11}$  for  $x = 0.4, 1.0,$  and  $1.6$  (Fig. 2a–c respectively).

In order to determine the type of transformation that recorded effects are due to, all the monophasic samples containing  $\text{Zn}_{2-x}\text{Mg}_x\text{FeV}_3\text{O}_{11}$  for  $0.2 \leq x \leq 1.8$  were additionally heated for 2 h at the temperatures corresponding to a half of the height of the registered endothermic effect. It was observed that all the samples were molten just as they were being taken out of the furnace. Thus, it can be concluded that the registered effects are due to the melting of the obtained solid solution. Figure 3 presents a phase diagram of the system  $\text{Zn}_2\text{FeV}_3\text{O}_{11}\text{--}\text{Mg}_2\text{FeV}_3\text{O}_{11}$  in subsolidus area. The new solid solution is stable up to the temperature of the solidus line.

**Fig. 2** Fragments of DTA curves of the solid solution  $\text{Zn}_{2-x}\text{Mg}_x\text{FeV}_3\text{O}_{11}$  for  $x = 0.4$  (curve a),  $x = 1.0$  (curve b),  $x = 1.6$  (curve c)

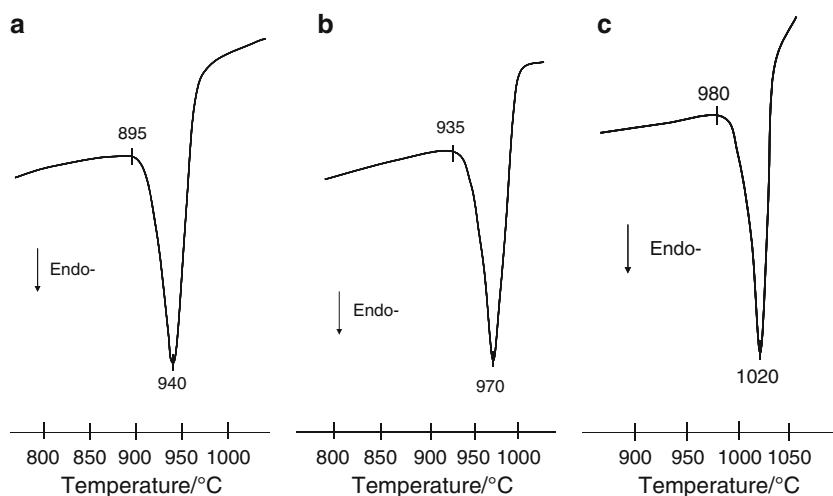


**Fig. 3** Phase diagram up to the solidus line of the system  $\text{Zn}_2\text{FeV}_3\text{O}_{11}$ – $\text{Mg}_2\text{FeV}_3\text{O}_{11}$

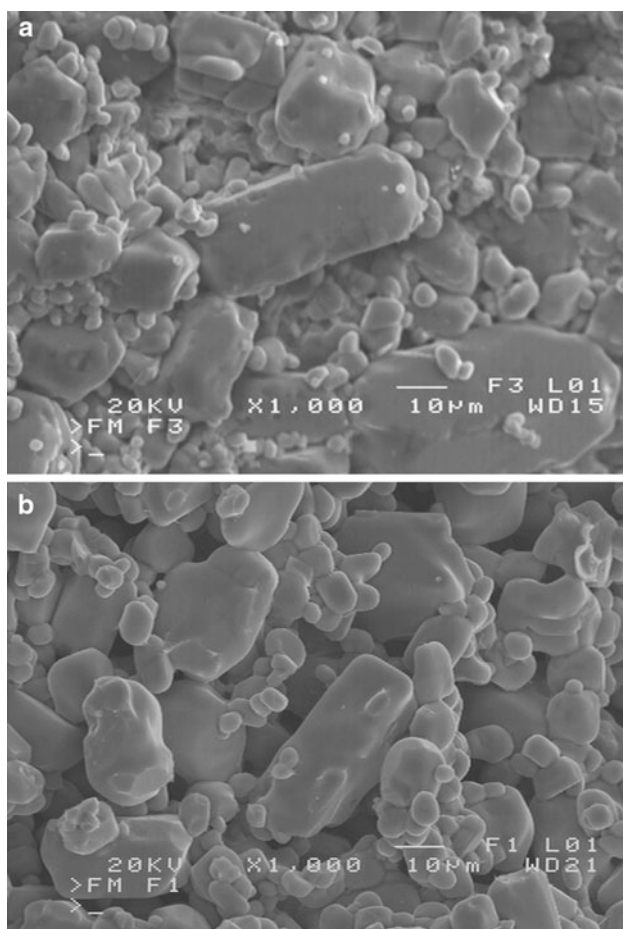
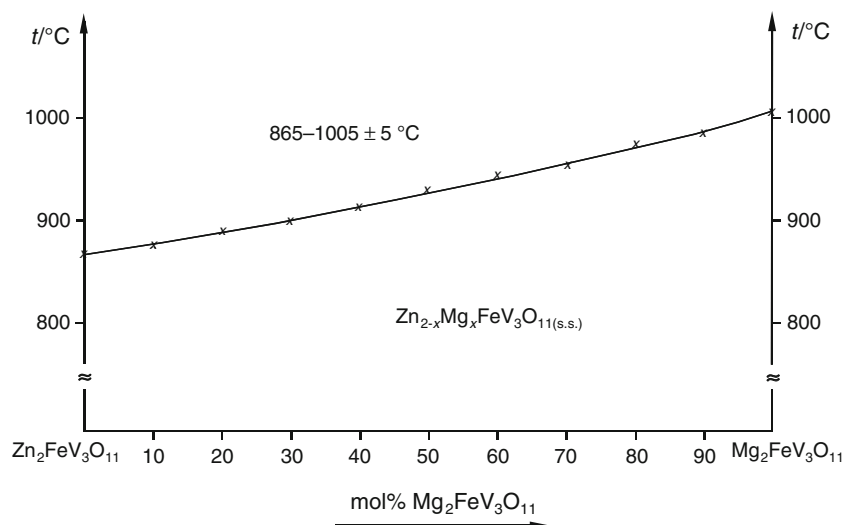


**Fig. 4** **a** SEM image of the solid solution with the formula  $\text{ZnMgFeV}_3\text{O}_{11}$ . **b** SEM image of the pure  $\text{Zn}_2\text{FeV}_3\text{O}_{11}$

#### SEM investigation

Figure 4a shows a scanning electron microscopic image of the new solid solution with the formula  $\text{ZnMgFeV}_3\text{O}_{11}$ ,

whereas Fig. 4b presents a SEM image of the matrix, i.e., pure  $\text{Zn}_2\text{FeV}_3\text{O}_{11}$ . The crystals showed in both of pictures are very similar in their morphology. They are very differentiated in size. The sizes of the larger crystals are of the order of 40  $\mu\text{m}$ , whereas the sizes of the smaller crystals do not often exceed 5  $\mu\text{m}$ .

#### Conclusions

The obtained results of research allow a statement that in the four-component oxide system, i.e.,  $\text{ZnO}$ – $\text{MgO}$ – $\text{Fe}_2\text{O}_3$ – $\text{V}_2\text{O}_5$ , a new solid solution of the formula  $\text{Zn}_{2-x}\text{Mg}_x\text{FeV}_3\text{O}_{11}$  is formed. This phase has been obtained by the conventional solid-state reaction technique using the starting mixtures containing  $\text{Zn}_2\text{FeV}_3\text{O}_{11}$  and  $\text{Mg}_2\text{FeV}_3\text{O}_{11}$ . Substitutional solid solution  $\text{Zn}_{2-x}\text{Mg}_x\text{FeV}_3\text{O}_{11}$  of a triclinic structure is formed in the whole concentration range of the  $\text{Zn}_2\text{FeV}_3\text{O}_{11}$ – $\text{Mg}_2\text{FeV}_3\text{O}_{11}$  subsystem (i.e., from  $x = 0$  to  $x = 2$ ). With increasing degree of  $\text{Mg}^{2+}$  ion incorporation into the  $\text{Zn}_2\text{FeV}_3\text{O}_{11}$  structure, the crystal lattice of the new phase contracts and positions of IR absorption bands shift to the higher wave numbers. The solid solution melts in the temperature range from  $865 \pm 5$  °C (for  $x = 0$ ) to  $1005 \pm 5$  °C (for  $x = 2$ ). The new phase may find applications in designing catalysts for various ODH (Oxidative Dehydrogenation) reactions.

**Open Access** This article is distributed under the terms of the Creative Commons Attribution License which permits any use, distribution, and reproduction in any medium, provided the original author(s) and the source are credited.

#### References

1. Korili SA, Ruiz P, Delmon B. Oxidative dehydrogenation of n-pentane on magnesium vanadate catalysts. *Catal Today*. 1996;32:229–35.

2. Jin M, Cheng Z-M, Gao Y-L, Fang X-C. Oxidative dehydrogenation of cyclohexane with  $\text{Mg}_3(\text{VO}_4)_2$  synthesized by the citrate process. *Mater Lett.* 2009;63:2055–8.
3. Owen OS, Kung MC, Kung HH. The effect of oxide structure and cation reduction potential of vanadates on the selective oxidative dehydrogenation of butane and propane. *Catal Lett.* 1992;12:45–50.
4. Blonska-Tabero A. A new iron lead vanadate  $\text{Pb}_2\text{FeV}_3\text{O}_{11}$ : synthesis and some properties. *Mater Res Bull.* 2009;44:1621–5.
5. Kurzawa M, Blonska-Tabero A, Rychlowska-Himmel I, Tabero P. Reactivity of  $\text{FeVO}_4$  towards oxides and pyrovanadates(V) of Co and Ni. *Mater Res Bull.* 2001;36:1379–90.
6. Kurzawa M, Blonska-Tabero A. Reactivity of  $\text{FeVO}_4$  towards  $\text{Zn}_2\text{V}_2\text{O}_7$ . *J Therm Anal Calorim.* 2003;72:145–50.
7. Rychlowska-Himmel I, Blonska-Tabero A. Studies on the system  $\text{ZnO-V}_2\text{O}_5\text{-Fe}_2\text{O}_3$ . Reactivity of  $\text{ZnFe}_2\text{O}_4$  towards  $\text{ZnV}_2\text{O}_6$ . *J Therm Anal Calorim.* 1999;56:205–10.
8. Guskos N, Wabia M, Kurzawa M, Beskrovnyi A, Likodimos V, Typek J, Rychlowska-Himmel I, Blonska-Tabero A. Neutron diffraction study of  $\text{Mg}_2\text{FeV}_3\text{O}_{11-\delta}$ . *Rad Eff Deff Solids.* 2003;158:369–74.
9. Wang X, Vander Griend DA, Stern ChL, Poepplmeier KR. Structure and cation distribution of new ternary vanadates  $\text{FeMg}_2\text{V}_3\text{O}_{11}$  and  $\text{FeZn}_2\text{V}_3\text{O}_{11}$ . *J Alloys Compd.* 2000;298:119–24.
10. Shannon RD. Revised effective ionic radii and systematic studies of interatomic distances in halides and chalcogenides. *Acta Cryst.* 1976;A32:751–67.
11. Tabero P, Filipek E. Synthesis and properties of the solid solutions formed in the  $\text{Fe}_2\text{V}_4\text{O}_{13}\text{-Cr}_2\text{V}_4\text{O}_{13}$  system. *J Therm Anal Calorim.* 2001;64:1067–72.
12. Tabero P, Filipek E. Synthesis and properties of a solid solution formed in the  $\text{CrVMoO}_7\text{-AlVMoO}_7$  system. *J Therm Anal Calorim.* 2004;77:183–91.
13. Tabero P, Filipek E. Synthesis and properties of solid solutions in the  $\text{FeVMoO}_7\text{-CrVMoO}_7$  system. *J Therm Anal Calorim.* 2001;64:1073–80.
14. Blonska-Tabero A, Bosacka M, Dabrowska G, Filipek E, Piz M, Rychlowska-Himmel I, Tabero P, Tomaszewicz E. The synthesis and properties of the phases obtained by solid–solid reactions. *J Min. Metall.* 2008;44B:19–26.
15. Filipek E, Piz M. The reactivity of  $\text{SbVO}_5$  with  $\text{T-Nb}_2\text{O}_5$  in solid state in air. *J Therm Anal Calorim.* 2010;101:447–53.
16. Šulcová P, Vitásková L, Trojan M. Thermal analysis of the  $\text{Ce}_{1-x}\text{Tb}_x\text{O}_2$  pigments. *J Therm Anal Calorim.* 2010;99:409–13.
17. Sawant P, Varma S, Wani BN, Bharadwaj SR. Influence of synthesis route on morphology and conduction behavior of  $\text{BaCe}_{0.8}\text{Y}_{0.2}\text{O}_{3-\delta}$ . *J Therm Anal Calorim.* 2012;107:189–95.
18. Roy M, Dave P, Barbar SK, Jangid S, Phase DM, Awasthi AM. X-ray, SEM, and DSC studies of ferroelectric  $\text{Pb}_{1-x}\text{Ba}_x\text{TiO}_3$  ceramics. *J Therm Anal Calorim.* 2010;101:833–7.
19. Šulcová P, Večeřa J, Bystrzycki P. Thermal analysis of doped  $\text{Bi}_2\text{O}_3$ . *J Therm Anal Calorim.* doi:10.1007/s10973-011-2135-z.
20. Tabero P. Formation and properties of the new  $\text{Al}_8\text{V}_{10}\text{W}_{16}\text{O}_{85}$  and  $\text{Fe}_{8-x}\text{Al}_x\text{V}_{10}\text{W}_{16}\text{O}_{85}$  phases with the  $\text{M-Nb}_2\text{O}_5$  structure. *J Therm Anal Calorim.* 2010;101:561–6.
21. Abello L, Husson E, Repelin Y, Lucazeau G. Vibrational spectra and valence force field of crystalline  $\text{V}_2\text{O}_5$ . *Spectrochim Acta.* 1983;39A:641–51.
22. Preudhomme J, Tarte P. Infrared studies of spinels-IV. Normal spinels with a high-valency tetrahedral cation. *Spectrochim Acta.* 1972;28A:69–79.
23. Dabrowska G, Tabero P, Kurzawa M. Phase relations in the  $\text{Al}_2\text{O}_3\text{-V}_2\text{O}_5\text{-MoO}_3$  system in the solid state. The crystal structure of  $\text{AlVO}_4$ . *J Phase Equilib Differ.* 2009;30:220–9.
24. Preudhomme J, Tarte P. Infrared studies of spinels-I. A critical discussion of the actual interpretations. *Spectrochim Acta.* 1971;27A:961–8.